An imager's guide to perineural tumor spread in head and neck cancers: radiological footprints

on 18F-FDG PET with CT and MRI correlates

Authors:

1) Hwan Lee, M.D.
2) Jillian W. Lazor, M.D
3) Reza Assadsangabi, M.D.
4) Jagruti Shah, M.D.

Affiliations:

Authors 1, 3, 4 - Division of Nuclear Medicine and Clinical Molecular Imaging, Department of Radiology, University of Pennsylvania, Philadelphia, PA

Author 2 - Division of Neuroradiology, Department of Radiology, University of Pennsylvania, Philadelphia, PA

Disclaimer: None

Corresponding author:

Name: Jagruti Shah, M.D.
Address: 3400 Spruce Street, Donner 110 A, Philadelphia, PA, 19104
Telephone: 215-662-3091
Fax: 215-349-5843
Email: Jagruti.shah4@gmail.com

First author:

Name: Hwan Lee, M.D.
Address: Department of Radiology, Hospital of the University of Pennsylvania, 3400 Spruce Street, Philadelphia, PA, 19104
Telephone: 484-515-0922
Fax: 215-349-5843
Email: Hwan.Lee@uphs.upenn.edu
Currently in training: Research fellow

Word count: 6773

Short Title: Head and neck perineural spread imaging

ABSTRACT

Perineural spread refers to tumor growth along large nerves, a macroscopic analogue of microscopic perineural invasion. This phenomenon most commonly occurs in head and neck, but its incidence varies with histologic tumor subtype. Perineural spread results from a complex molecular interplay between tumor cells, nerves, and connective stroma. Perineural spread is clinically underdiagnosed despite its impact on patients' prognosis and management. The role of 18F-fluorodeoxyglucose positron emission tomography (18F-FDG PET) in assessment of perineural spread in head and neck cancer remains to be explored, in contrast to magnetic resonance imaging (MRI) as the established gold standard. In patients with perineural spread, 18F-FDG PET shows both abnormality along the course of the involved nerve and muscular changes secondary to denervation. Assessment of perineural spread on 18F-FDG PET requires knowledge of relevant neural pathways, and it can be improved by correlation with anatomic imaging, additional image processing, and review of clinical context.

Key Words

Perineural spread, head and neck cancer, cranial nerves, 18F-FDG PET, correlative imaging

INTRODUCTION

The term head and neck cancer encompasses a heterogeneous group of malignancies occurring in the oral, sinonasal, pharyngeal, and laryngeal mucosa, as well as in the salivary glands and skin of head and neck (*1*). Diagnosis and management of head and neck cancer often involves 18F-fluorodeoxyglucose (FDG) positron emission tomography/computed tomography (PET/CT) imaging for a variety of roles including unknown primary tumor detection, staging, radiation therapy planning, response assessment, and post-treatment surveillance (*2*).

Head and neck cancer can spread by direct extension or by hematogenous or lymphatic routes (*3*). An additional means of spread is extension of tumor along nerves, a phenomenon called perineural tumor growth (*3*). Imaging is critical in diagnosis of perineural tumor growth: clinical underdiagnosis is common as up to 40% of the affected patients are asymptomatic (*4*).

Although the sensitivity and specificity of magnetic resonance imaging (MRI) in assessment of perineural tumor growth have been characterized (*5-7*), there is limited data on accuracy of 18F-FDG PET in detection of perineural tumor growth (*3*). The aim of this article is to increase awareness of perineural spread in head and neck cancer and describe imaging findings of perineural spread with focus on 18F-FDG PET. We summarize the pathogenesis, clinical implications, and pattern of perineural spread with emphasis on neuroanatomy and primary and secondary imaging findings of perineural spread on both metabolic and anatomic imaging.

DEFINITION AND INCIDENCE

Extension of neoplasm along the course of a nerve is termed perineural tumor growth, which is divided into two types: perineural invasion (PNI) and perineural spread (PNS). PNI refers to tumor invasion into the neural space of small, unnamed nerve branches confined to the main tumor site, whereas PNS involves larger, named nerves often accompanied with distant tumor spread along the nerves away from the primary site (*8*). Unlike PNI, PNS is evident on imaging and can be discovered by clinical manifestations directly related to the involved nerve (*7*).

Most of the data available for incidence and prevalence of perineural growth of head and neck tumors refers to PNI rather than PNS. Regardless of the choice of terminology, relative comparison of propensity for nerve involvement among different histologic tumor types remains informative.

The overall reported incidence of PNI in head and neck cancers varies widely from 2.5%-80%, as frequency varies with the tumor histologic type and location of primary tumor (*9,10*). The rates of PNI for various histologic types are summarized on Supplemental Table 1 (*11-23*). The risk for PNS increases with mid-face location of the tumor, larger tumor size, male gender, poor histologic differentiation, and with recurrent tumor (*24*). The evaluation and interpretation of suspected imaging findings of PNS can be improved by accounting for the histologic type, location of the primary tumor and careful evaluation of certain anatomic sites which are more conducive to neural involvement, such as the masticator space, pterygopalatine fossa, Meckel's cave or cavernous sinus (*3,10,25,26*).

PATHOGENIC MECHANISM

The most current and widely accepted model of perineural tumor growth is based on a complex biochemical interaction between the tumor cells and nerve microenvironment (*8*). The functional outcomes of the biochemical interactions include stromal manipulation, neurotropism, neurite production, and nerve-tumor adhesion (Fig. 1) (*8,27*). To date, a number of proteins have been discovered to play a role (Fig. 1). The full biochemical landscape remains to be explored, with ongoing discovery of increasingly more mechanisms such as nerve-initiated immune response (*28*).

Differences in the biochemical profile of tumors can explain the variation in their propensity for perineural growth. For example, desmoplastic melanoma, a type of melanoma with high rates of PNI (Supplemental Table 1), exhibits a higher expression of nerve growth factor receptor, a protein involved in PNS (*29*). Continued research on the pathogenesis of perineural tumor growth can lead to potential therapeutic targets. For example, blockade of tropomyosin receptor kinases, involved in PNS signaling (*30*), has reached up to phase II clinical trial with promising results in patients with various tumor types, including head and neck cancers (*31*).

CLINICAL SIGNIFICANCE

Perineural involvement of tumor impacts prognosis, risk stratification, staging, and treatment planning. The prognostic value of perineural involvement varies depending on the histologic subtype of the tumor and the site of primary malignancy. In general, perineural disease confers a higher risk of local recurrence, a higher risk of metastasis, and poorer survival.

In mucosal head and neck squamous cell carcinoma (HNSCC) (all subsites), PNI is associated with increased local recurrence (23% vs. 9%) and worse disease-specific mortality (54% vs. 25%) (*32*). PNI has also been found to be a predictor of lymph node metastases (*32*). PNI is a predictor of distant recurrence, in addition to worse disease-free survival, in oral tongue squamous cell carcinoma (*33*). In cutaneous HNSCC, symptomatic versus asymptomatic patients with PNI have significantly worse rate of 10-year local control (50% vs. 78%) (*24*).

Poor prognosis has been observed in salivary gland cancers with PNI. In patients with mucoepidermoid carcinoma, PNI was associated with a decreased 5-year disease-free survival (57.7% vs. 88.8%) (*17*). In adenoid cystic carcinoma, PNI was associated with a higher rate of recurrence (81.8% vs. 26.7%), a higher rate of distant metastases (40% vs. 0%), and lower 5-year survival (36.9% vs. 93.8%) (*34*).

Fewer studies have explored the prognostic implications of PNS as detected on imaging. Williams et al. found that patients with cutaneous squamous cell and basal cell carcinoma with and without PNS on imaging had significantly worse 5-year local control rates (35% vs. 78%), 5-year overall survival (50 % vs. 86%) and 5-year cause-specific survival (54% vs. 94%) (*35*). Balamucki et al. found a significant difference in 5-year disease-specific survival in patients with and without radiographic evidence of PNS in cutaneous HNSCC (*24*).

These prognostic implications are important for clinical management and treatment planning. With regards to the site of primary tumor, the goal of surgical excision is complete resection of tumor and the involved extracranial nerve. Intracranial extension of PNS deems a patient inoperable, due to the risk of central nervous system seeding of tumor. These patients are often treated with palliative radiation (*36)*, with surgery performed on case-by-case basis with

the goal of tumor debulking to improve efficacy of adjuvant therapy and patient symptoms (*37*). The 2018 National Comprehensive Cancer Network guidelines recommend post-surgical adjuvant radiation for mucosal HNSCC, salivary gland carcinoma, and melanoma with PNI (*38,39*), as well for cutaneous squamous cell and basal cell carcinoma with extensive or large nerve PNI (*40,41*).

PERINEURAL PATHWAYS

PNS in head and neck cancers can occur along any cranial nerve (CN). The most commonly involved cranial nerves in PNS are the maxillary and mandibular division of the trigeminal nerve (CN V2 and V3, respectively) and the facial nerve (CN VII) because of their widespread innervation of the head and neck structures (*1*). The ophthalmic division of the trigeminal nerve (CN V1) and the hypoglossal nerve (CN XII) are less frequently involved (*10*). Primary tumor sites for the cranial nerves commonly involved in PNS are summarized on Supplemental Table 2.

Tumors may spread from one cranial nerve to another because of their close proximity or communication between their peripheral branches, particularly between CN V and VII. There are at least few different locations of their interconnections: 1) CN VII fibers, via the greater superficial petrosal nerve, communicate with small CN V2 branches in the pterygopalatine ganglion; 2) Chorda tympani, a branch of CN VII, joins with lingual nerve, a branch of CN V3; 3) CN VII communicates with the auriculotemporal nerve, a branch of V3 in the parotid gland (*42-44*). Other regions of cranial nerve interconnection include CN V1 and V2 in the cavernous sinus and CN V1, V2 and V3 in Meckel's cave (*1,4*).

While interpreting an imaging study on patient with known or suspected head and neck cancer, one should have knowledge of cranial nerve anatomy, closely scrutinize the entire course of cranial nerves in proximity to the primary tumor, and evaluate the course of the interconnecting cranial nerves. In multiple cranial neuropathies, one should suspect tumor spread to the skull base, PNS to anatomic courses conducive for multiple nerve involvement, or leptomeningeal carcinomatosis (*14*). The continuity between the perineurium and leptomeninges in the intracranial segments of cranial nerves permits leptomeningeal spread of tumor cells (*14*).

CLINICAL FEATURES

Approximately 40% of patients with PNS of tumor in head and neck cancers are asymptomatic (*4*). The signs and symptoms most commonly associated with PNS are facial pain, paresthesia, numbness, and weakness of the muscles of mastication and facial expression, as branches of the trigeminal and facial nerves are the most commonly involved cranial nerves in PNS (*10,26,45*). Such signs and symptoms can direct the interpreting physician's attention to the cranial nerves responsible for the neurologic deficit (Supplemental Table 3).

IMAGING FEATURES

It is well established that imaging plays a key role in assessment and management of head and neck malignancies. Little data exists regarding the diagnostic performance of 18F-FDG PET/CT for detection of PNS of head and neck cancer, the reason being multifactorial: the interpreting physician's lack of suspicion or familiarity with the relevant imaging findings,

confounding treatment-related uptake in post-therapy patients, relatively lower spatial resolution of 18F-FDG PET images, and obscuration of findings by physiologic brain uptake at the skull base. One case-control study reported a PNS detection rate of 100% for 18F-FDG PET/CT, though this is likely an overestimate of the performance in the general clinical setting, as the PET scans in this study were interpreted in light of MRI and tumor board consensus findings of PNS (*46*).

MRI is the modality of choice when evaluating PNS, offering superior soft tissue contrast and fewer artifacts from dental hardware compared to CT (*26*). Sensitivity and specificity of MRI for detection of PNS is 95%-100% (*5-7*) and 85% respectively (*5,6*). However, the sensitivity of MRI to demonstrate the full extent of anatomic distribution of PNS is lower at 63%-89% (*5,7*). In comparison, the sensitivity and specificity of CT for detection of PNS are 88% and 89%, respectively (*6*).

In our experience, both PET and conventional imaging modalities (MRI and CT) should be regarded as complementary in assessment of PNS, and the full extent of PNS can be best appreciated with identification of both structural and metabolic imaging findings. (Supplemental Table 3).

Primary Imaging Findings

On anatomic imaging, PNS appears as thickening, nodularity, and enhancement of the involved cranial nerve (*47,48*). Infiltration or obliteration of fat in the deep spaces of the face and at the skull base foramina is a sensitive indicator of PNS. Enlargement or erosion of skull base foramina is suggestive of PNS, better evaluated on CT than MRI (Fig. 2F) (*47*).

The primary imaging feature of PNS on 18F-FDG PET/CT is linear or curvilinear

increased FDG uptake along the distribution of the cranial nerve relative to activity of the surrounding tissue, which may be continuous or discontinuous with the primary tumor (*25*). While interpreting 18F-FDG PET/CT in head and neck cancer, one must assess all three standard imaging planes and maximum intensity projection (MIP) images of the PET to evaluate for PNS. MIP technique helps fully visualize the extent of PNS over the non-planar anatomic course of the involved nerves (Fig. 2A,3A,4C).

Another technique for improved assessment of PNS on 18F-FDG PET/CT is evaluation of the concurrently obtained CT images for the above described findings. If available, retrospective evaluation, correlation or fusion of the PET images with a recently acquired higher resolution CT (Fig. 5B-C) or contrast-enhanced MRI (Fig. 3C) could also be performed to improve the anatomic localization.

Secondary Imaging Findings

If PNS causes damage to a motor branch of a cranial nerve, the denervated musculature undergoes flaccid paresis and eventual atrophy. During the acute phases, there is hyperintense signal and abnormal muscle enhancement on T2-weighted and fat suppressed post-contrast T1-weighted images respectively on MRI and muscle edema on the CT (*49*). On 18F-FDG PET, one may detect increased FDG uptake in the affected musculature in the early acute phase which normalizes in the later stages (*50*). In chronic phase, there is muscle atrophy with decreased FDG uptake in the affected musculature on PET and volume loss with fatty replacement on CT and MRI (*25,49*). On 18F-FDG PET, a dominant finding may also be increased conspicuity of physiologic or compensatory uptake in the contralateral unaffected musculature, such as in the contralateral tongue or vocal cord in the case of CN XII or X denervation, respectively (*25*).

Potential Imaging Pitfalls

One must also be cautious while reviewing 18F-FDG PET/CT in head and neck cancers. Altered anatomic landmarks after treatment and asymmetric physiologic uptake can often make image interpretation challenging.

The uptake intensity along the nerve course may be subtle, leading to a false-negative scan. Other reasons for false-negative scan can be improper PET/CT image co-registration because of motion and high adjacent background activity in the brain, which can compromise the evaluation of PNS at the skull base foramina. Also, partial volume effect and insufficient spatial resolution for smaller lesions (<1 cm) can limit the sensitivity of PET for PNS detection, particularly for smaller nerve branches, unless there is significantly increased FDG uptake that contrasts with low background activity (*51*).

False-positive scans can be seen secondary to inflammation from post-radiation or postsurgical changes, particularly when the 18F-FDG PET/CT is performed within 1 month of surgery, chemotherapy or radiation therapy. The current consensus is that 18F-FDG PET/CT should be deferred until at least 12 weeks after chemoradiation therapy to allow resolution of treatment-related changes (*52*). Asymmetric physiologic FDG uptake in the neck muscles and variable physiologic uptake in normal structures such as masticator muscles, extraocular muscles, and lymphoid tissue such as Waldyer's ring can also be confounding factors. A review of CT portion of PET/CT allows correlation of findings with normal anatomic structures, thus reducing the false-positive findings. Some of the mimics of PNS are certain FDG-avid neurogenic tumors and rarely meningioma protruding through skull base foramina. There are reports of PNS associated with other non-neoplastic diseases such as mucormycosis, invasive

aspergillosis, and sinonasal sarcoidosis (*4,18*). Careful assessment of the patient history, physical examination findings, correlative imaging, and histologic information can help avoid such pitfalls.

CRANIAL NERVE ANATOMY AND PNS IMAGING FEATURES

The trigeminal, facial, and hypoglossal nerves, the most commonly involved cranial nerves with PNS, are described first (Supplemental Fig. 1,2), followed by the other less commonly involved cranial nerves.

Trigeminal Nerve (CN V)

The trigeminal nerve emerges from the pons, forms the trigeminal ganglion at the Meckel's cave in the middle cranial fossa, and then splits into three main divisions: the ophthalmic (CN V1), maxillary (CN V2), and mandibular nerves (CN V3) (*45*).

Mandibular Division of Trigeminal Nerve (CN V3)

The mandibular nerve is a mixed sensory and motor nerve, supplying the muscles of mastication (*53*). From the trigeminal ganglion, the mandibular nerve travels inferiorly through foramen ovale to exit the skull base and enter the masticator space (*45,53*). It then divides into the mostly sensory anterior (deep temporal, lateral pterygoid, masseteric, and buccal nerves) and mostly motor posterior (auriculotemporal, lingual, and inferior alveolar nerves) trunks (*53*).

Tumors that can spread along the mandibular nerve (CN V3) include lower lip and chin skin cancer (Fig. 2A-C), neoplasms involving the anterior two thirds of the tongue and floor of mouth, periauricular and temporal cutaneous or parotid malignancy, and neoplasms originating

from the masticator space, nasopharynx, or oropharynx (*4*).

PNS along the mandibular division can be suspected when abnormal linear FDG uptake on 18F-FDG PET/CT is seen within the mandibular canal along the inferior alveolar nerve (Fig. 2C), on the medial mandibular surface (*3*), or in the masticator space (Fig. 2D). The abnormal FDG uptake can further extend superiorly to reach foramen ovale (Fig. 2E) or Meckel's cave (Fig. 2G). The CT or MRI may show enlargement of the neural foramina (mental, mandibular, or ovale) (Fig. 2F). In addition, secondary signs of ipsilateral masticator muscle denervation injury may be identified on imaging.

Maxillary Division of Trigeminal Nerve (CN V2)

The maxillary nerve, a somatic sensory nerve, travels from the trigeminal ganglion anteriorly across the cavernous sinus and through foramen rotundum into the pterygopalatine fossa (*53*). It then enters the orbit via the inferior orbital fissure, travels within the infraorbital groove and canal, and then exits the skull through the infraorbital foramen to innervate the facial skin (*54*). From the maxillary nerve also emerge the middle meningeal, zygomatic, and superior alveolar nerves, as well as the pterygopalatine ganglion where multiple mucosal branches originate (*54*).

PNS along the maxillary nerve most commonly occurs along the mucosal branches by HNSCC or adenoid cystic carcinoma (ACC) in the oral cavity, pharynx, palate or sinonasal tract (*26*). Skin malignancy around the cheek, nose or upper lip, especially squamous cell carcinoma or desmoplastic melanoma, can also spread along the maxillary nerve (*3*).

PNS along the maxillary nerve can be suspected when a mucocutaneous FDG-avid lesion extends to the infraorbital canal or pterygopalatine fossa and potentially further into foramen

rotundum or the cavernous sinus (Fig. 3). CT or MRI may also identify obliteration of the fat within pterygopalatine fossa and enlargement of the infraorbital foramen, inferior orbital fissure, or foramen rotundum (Fig. 3).

Ophthalmic Division of Trigeminal Nerve (CN V1)

The ophthalmic nerve, a somatic sensory nerve, arises from the trigeminal ganglion in Meckel's cave. It travels anteriorly across the cavernous sinus and splits into the frontal, lacrimal, and nasociliary nerves just before entering the orbit through the superior orbital fissure (*55*). The frontal nerve is the largest branch and exits the orbit to innervate the upper facial skin (*55*).

PNS along the ophthalmic nerve (CN V1) most commonly occurs due to skin cancers of the upper face that invade the frontal nerve branches, and less commonly by intraorbital or sinonasal neoplasms involving the nasoethmoid complex (*10*).

The small caliber of the cranial nerves within the orbit (except the optic nerve) make it difficult to visualize their involvement on 18F-FDG PET (*25*). Nevertheless, PNS along the ophthalmic nerve can be suspected when a periorbital cutaneous neoplasm makes a seemingly non-contiguous spread to the orbital apex (Fig. 5B). CT/MRI may show direct nerve involvement on high resolution images (Fig. 5A) or enlargement of the optic canal or superior orbital fissure at the orbital apex. CN III, IV and VI may become involved with PNS as they share a common pathway with CN V1 in the cavernous sinus and into the orbit. Decreased FDG uptake or atrophy of the extraocular muscles (Fig. 5B-C) is a useful secondary indicator of PNS.

Facial Nerve (CN VII)

The facial nerve innervates the muscles of facial expression (*56*) and also carries taste afferents from the anterior two-thirds of the tongue (*56*). It arises from the brainstem at the lower pons, enters the internal acoustic canal along with the vestibulocochlear nerve, traverses through the meatal foramen into the facial canal, and then continues sequentially as the labyrinthine segment, geniculate ganglion, tympanic segment, and mastoid segment before exiting the skull through the stylomastoid foramen (*56*). It then enters the parotid gland and splits into the five terminal branches that innervate the muscles of facial expression (*57*). From the geniculate ganglion also emerges the greater superficial petrosal nerve carrying the parasympathetic fibers, joining branches of the maxillary nerve (CN V2) at the pterygopalatine ganglion (*57*).

PNS along the facial nerve most commonly occurs in primary parotid malignancy or through neoplasm from the adjacent skin invading the parotid gland (*1,26*). Tumor can spread cephalad from the parotid gland, with abnormal FDG activity at the stylomastoid foramen and mastoid segment of the temporal bone (Fig. 6) or stylomastoid foramen enlargement on anatomic imaging raising suspicion for PNS. Another commonly involved neural pathway is along the greater superficial petrosal nerve by a neoplasm reaching the pterygopalatine ganglion, for example a hard palate ACC (*10*).

Hypoglossal Nerve (CN XII)

The hypoglossal nerve controls the muscles of the tongue (*58*). Emerging from the medulla, the hypoglossal nerve travels through the hypoglossal canal and down the carotid space (*58*). At the level of the angle of the mandible, it turns anteriorly to reach the muscles of the tongue (*58*). The cervical course of the hypoglossal nerve in the carotid space is in close

proximity to the cranial nerves IX, X and XI.

PNS along the hypoglossal nerve is most commonly caused by posterolateral extension of nasopharyngeal carcinoma (*10*). Retrograde spread from a tongue base or sublingual space malignancy (*57,58*) or metastatic carotid space tumor may also occur, shown as abnormal FDG-avid lesion tracking superiorly along the carotid space to the hypoglossal canal on 18F-FDG PET/CT (Fig. 4). Potential secondary imaging findings of PNS along the hypoglossal nerve include decreased FDG activity and atrophy/fatty replacement of the ipsilateral tongue as late stage of denervation injury on 18F-FDG PET/CT (Fig. 4D) and MRI, as well as hypoglossal canal enlargement on anatomic imaging.

Olfactory Nerve (CN I)

The olfactory nerve carries the sense of smell from the nasal mucosa (*59*). The olfactory nerve refers to bundles of axons that originate from the olfactory bulb and pass through the numerous olfactory foramina in the cribriform plate of the ethmoid bone (*59*). Although direct visualization of the olfactory nerve is beyond the resolution of 18F-FDG PET (*25*), PNS should be suspected when the cribriform plate is involved with lesions in superior sinonasal and anterior cranial fossa region by tumors such as esthesioneuroblastoma, sinonasal squamous cell carcinoma and melanoma (Supplemental Fig. 3).

Optic, Oculomotor, Trochlear and Abducens Nerves (CN II, III, IV, VI)

The optic nerve originates from the optic chiasm and enters the orbit via the optic canal, innervating the retina to carry visual sensory information (*59*). The oculomotor, trochlear, and abducens nerves control the extraocular muscles and arise from the brainstem. PNS along the CN V1 can involve any of these other cranial nerves in the orbit as they share a similar course along

the cavernous sinus into the superior orbital fissure and the orbit. Focal increased FDG uptake in the orbital apex or cavernous sinus with secondary findings of extraocular muscle atrophy should raise suspicion for cranial nerves III, IV or VI involvement in a patient with periorbital neoplasm (Fig. 5).

Vestibulocochlear Nerve (CN VIII)

The vestibulocochlear nerve is responsible for sensation of hearing and rotational/linear acceleration (*60*). It emerges from the pontomedullary junction and enters the internal acoustic canal alongside the facial nerve and innervates the cochlear and vestibular apparatus within the petrous part of the temporal bone (*60*).

Perineural involvement of the vestibulocochlear nerve can occur when PNS of head and neck cancer along the facial nerve has extended cephalad past the geniculate ganglion into its canalicular segment, where the CN VII and CN VIII are in close proximity. The imaging findings of linear increased FDG uptake in the internal acoustic canal on 18F-FDG PET/CT or destruction of bony labryinth or enlargement of the internal acoustic canal on CT or MRI should also raise suspicion for vestibulocochlear nerve involvement in a patient with PNS involving facial nerve presenting with new symptoms of hearing loss or imbalance (Supplemental Fig. 4).

Glossopharyngeal, Vagus, and Accessory Nerves (CN IX, X, XI)

The glossopharyngeal nerve supplies efferent fibers to the stylopharyngeus muscle and parotid gland, while also receiving sensory input from the pharyngeal mucosa, palatine tonsil, carotid body, and posterior one-third of the tongue (*61*). The vagus nerve carries motor fibers to the muscles of the larynx and pharynx responsible for speech and swallowing, along with sensory fibers from the same areas (*61*). It also provides visceral sensory and parasympathetic

motor innervation to thorax and abdomen (*61*). The accessory nerve innervates the sternocleidomastoid and trapezius muscles (*61*).

The glossopharyngeal, vagus, and accessory nerves share their anatomic course through the jugular foramen at the skull base and down the carotid space (*59,61*). Therefore, a head and neck neoplasm extending to the carotid space can subsequently spread variably along these three cranial nerves to reach the jugular foramen, visible as abnormal focal or linear increased FDG uptake along their course in the lateral neck and jugular foramen on 18F-FDG PET (Supplemental Fig. 5). There may be enhancement along the nerve course on T1-weighted post-contrast MRI and widening or destructive bony changes in the jugular foramen on CT. End-organ dysfunction will result in paralysis of pharyngeal and soft palate muscles secondary to involvement of glossopharyngeal and vagus nerve, vocal cord paralysis with involvement of recurrent laryngeal branch of vagus nerve (Supplemental Fig. 6A), and paralysis of sternocleidomastoid and trapezius muscle with accessory nerve involvement (Supplemental Fig. 6B).

CONCLUSION

PNS is an important neoplastic feature that needs to be considered and recognized on imaging with impact on patients' prognosis and management. 18F-FDG PET can identify PNS of head and neck malignancies along the cranial nerves. Correlation or fusion of PET with CT or MRI improves assessment of both the presence and extent of perineural spread. In addition to knowledge of the imaging findings and associated neuroanatomy, further image processing and review of the clinical context can improve interpretation of suspected cases of PNS. The advent

of PET/MR in clinical practice may provide further enhancement in detection of PNS in head and neck tumors.

DISCLOSURE

REFERENCES

1.   Ginsberg LE. Imaging of perineural tumor spread in head and neck cancer. *Semin Ultrasound CT MR.* 1999;20:175-186.

2.   Subramaniam RM, Truong M, Peller P, Sakai O, Mercier G. Fluorodeoxyglucose-positron-emission tomography imaging of head and neck squamous cell cancer. *AJNR Am J Neuroradiol.* 2010;31:598-604.

3.   Paes FM, Singer AD, Checkver AN, Palmquist RA, De La Vega G, Sidani C. Perineural spread in head and neck malignancies: clinical significance and evaluation with 18F-FDG PET/CT. *Radiographics.* 2013;33:1717-1736.

4.   Gandhi D, Gujar S, Mukherji SK. Magnetic resonance imaging of perineural spread of head and neck malignancies. *Top Magn Reson Imaging.* 2004;15:79-85.

5.   Baulch J, Gandhi M, Sommerville J, Panizza B. 3T MRI evaluation of large nerve perineural spread of head and neck cancers. *J Med Imaging Radiat Oncol.* 2015;59:578-585.

6.   Hanna E, Vural E, Prokopakis E, Carrau R, Snyderman C, Weissman J. The sensitivity and specificity of high-resolution imaging in evaluating perineural spread of adenoid cystic carcinoma to the skull base. *Arch Otolaryngol Head Neck Surg.* 2007;133:541-545.

7.   Nemzek WR, Hecht S, Gandour-Edwards R, Donald P, McKennan K. Perineural spread of head and neck tumors: how accurate is MR imaging? *AJNR Am J Neuroradiol.* 1998;19:701-706.

8.   Brown IS. Pathology of perineural spread. *J Neurol Surg B Skull Base.* 2016;77:124-130.

9.   Marchesi F, Piemonti L, Mantovani A, Allavena P. Molecular mechanisms of perineural invasion, a forgotten pathway of dissemination and metastasis. *Cytokine Growth Factor Rev.* 2010;21:77-82.

10.   Maroldi R, Farina D, Borghesi A, Marconi A, Gatti E. Perineural tumor spread. *Neuroimaging Clin N Am.* 2008;18:413-429, xi.

11.   Roh J, Muelleman T, Tawfik O, Thomas SM. Perineural growth in head and neck squamous cell carcinoma: a review. *Oral Oncol.* 2015;51:16-23.

12.   Blanchard P, Baujat B, Holostenco V, et al. Meta-analysis of chemotherapy in head and neck cancer (MACH-NC): a comprehensive analysis by tumour site. *Radiother Oncol.* 2011;100:33-40.

13.   Chirila M, Bolboaca SD, Cosgarea M, Tomescu E, Muresan M. Perineural invasion of the major and minor nerves in laryngeal and hypopharyngeal cancer. *Otolaryngol Head Neck Surg.* 2009;140:65-69.

14.   Dunn M, Morgan MB, Beer TW. Perineural invasion: identification, significance, and a standardized definition. *Dermatol Surg.* 2009;35:214-221.

15.   Alam M, Ratner D. Cutaneous squamous-cell carcinoma. *N Engl J Med.* 2001;344:975-983.

16.   Hassanein AM, Proper SA, Depcik-Smith ND, Flowers FP. Peritumoral fibrosis in basal cell and squamous cell carcinoma mimicking perineural invasion: potential pitfall in Mohs micrographic surgery. *Dermatol Surg.* 2005;31:1101-1106.

17.   McHugh CH, Roberts DB, El-Naggar AK, et al. Prognostic factors in mucoepidermoid

carcinoma of the salivary glands. *Cancer.* 2012;118:3928-3936.

18. Ronaghy A, Yaar R, Goldberg LJ, Mahalingam M, Bhawan J. Perineural involvement: what does it mean? *Am J Dermatopathol.* 2010;32:469-476.

19. Yu JB, Blitzblau RC, Patel SC, Decker RH, Wilson LD. Surveillance, Epidemiology, and End Results (SEER) database analysis of microcystic adnexal carcinoma (sclerosing sweat duct carcinoma) of the skin. *Am J Clin Oncol.* 2010;33:125-127.

20. Chang PC, Fischbein NJ, McCalmont TH, et al. Perineural spread of malignant melanoma of the head and neck: clinical and imaging features. *AJNR Am J Neuroradiol.* 2004;25:5-11.

21. Barrett AW, Speight PM. Perineural invasion in adenoid cystic carcinoma of the salivary glands: A valid prognostic indicator? *Oral Oncol.* 2009;45:936-940.

22. Naylor E, Sarkar P, Perlis CS, Giri D, Gnepp DR, Robinson-Bostom L. Primary cutaneous adenoid cystic carcinoma. *J Am Acad Dermatol.* 2008;58:636-641.

23. Dores GM, Huycke MM, Devesa SS, Garcia CA. Primary cutaneous adenoid cystic carcinoma in the United States: incidence, survival, and associated cancers, 1976 to 2005. *J Am Acad Dermatol.* 2010;63:71-78.

24. Balamucki CJ, Mancuso AA, Amdur RJ, et al. Skin carcinoma of the head and neck with perineural invasion. *Am J Otolaryngol.* 2012;33:447-454.

25. Raslan OA, Muzaffar R, Shetty V, Osman MM. Image findings of cranial nerve pathology on [18F]-2-deoxy-D-glucose (FDG) positron emission tomography with computerized tomography (PET/CT): a pictorial essay. *Cancer Imaging.* 2015;15:20.

26. Amit M, Eran A, Billan S, et al. Perineural spread in noncutaneous head and neck cancer: new insights into an old problem. *J Neurol Surg B Skull Base.* 2016;77:86-95.

27. Bakst RL, Wong RJ. Mechanisms of perineural invasion. *J Neurol Surg B Skull Base.* 2016;77:96-106.

28. Bakst RL, Xiong H, Chen CH, et al. Inflammatory monocytes promote perineural invasion via CCL2-mediated recruitment and cathepsin B expression. *Cancer Res.* 2017;77:6400-6414.

29. Ohsie SJ, Sarantopoulos GP, Cochran AJ, Binder SW. Immunohistochemical characteristics of melanoma. *J Cutan Pathol.* 2008;35:433-444.

30. Amatu A, Sartore-Bianchi A, Siena S. NTRK gene fusions as novel targets of cancer therapy across multiple tumour types. *ESMO Open.* 2016;1:e000023.

31. Drilon A, Laetsch TW, Kummar S, et al. Efficacy of larotrectinib in TRK fusion-positive cancers in adults and children. *N Engl J Med.* 2018;378:731-739.

32. Fagan JJ, Collins B, Barnes L, D'Amico F, Myers EN, Johnson JT. Perineural invasion in squamous cell carcinoma of the head and neck. *Arch Otolaryngol Head Neck Surg.* 1998;124:637-640.

33. Cracchiolo JR, Xu B, Migliacci JC, et al. Patterns of recurrence in oral tongue cancer with perineural invasion. *Head Neck.* 2018;40:1287-1295.

34. Vrielinck LJ, Ostyn F, van Damme B, van den Bogaert W, Fossion E. The significance of perineural spread in adenoid cystic carcinoma of the major and minor salivary glands. *Int J Oral Maxillofac Surg.* 1988;17:190-193.

35. Williams LS, Mancuso AA, Mendenhall WM. Perineural spread of cutaneous squamous and basal cell carcinoma: CT and MR detection and its impact on patient management and prognosis. *Int J Radiat Oncol Biol Phys.* 2001;49:1061-1069.

36. Warren TA, Panizza B, Porceddu SV, et al. Outcomes after surgery and postoperative radiotherapy for perineural spread of head and neck cutaneous squamous cell carcinoma. *Head Neck.* 2016;38:824-831.

37. Palejwala SK, Barry JY, Rodriguez CN, Parikh CA, Goldstein SA, Lemole GM, Jr. Combined approaches to the skull base for intracranial extension of tumors via perineural spread can improve patient outcomes. *Clin Neurol Neurosurg.* 2016;150:46-53.

38. NCCN clinical practice guidelines in oncology: head and neck cancers (Version 1.2018). National Comprehensive Cancer Network website. https://www.nccn.org/professionals/physician_gls/pdf/head-and-neck.pdf. Updated February 15, 2018. Accessed June 9, 2018.

39. NCCN clinical practice guidelines in oncology: melanoma (Version 2.2018). National Comprehensive Cancer Network website. https://www.nccn.org/professionals/physician_gls/PDF/melanoma.pdf. Updated January 19, 2018. Accessed June 9, 2018.

40. NCCN clinical practice guidelines in oncology: squamous cell skin cancer (Version 2.2018). National Comprehensive Cancer Network website. https://www.nccn.org/professionals/physician_gls/pdf/squamous.pdf. Updated October 5, 2017. Accessed June 9, 2018.

41.   NCCN clinical practice guidelines in oncology: basal cell skin cancer (Version 1.2018). National Comprehensive Cancer Network website. https://www.nccn.org/professionals/physician_gls/pdf/nmsc.pdf. Updated September 18, 2017. Accessed June 9, 2018.

42.   Schmalfuss IM, Tart RP, Mukherji S, Mancuso AA. Perineural tumor spread along the auriculotemporal nerve. *AJNR Am J Neuroradiol.* 2002;23:303-311.

43.   Ginsberg LE, De Monte F, Gillenwater AM. Greater superficial petrosal nerve: anatomy and MR findings in perineural tumor spread. *AJNR Am J Neuroradiol.* 1996;17:389-393.

44.   Bagatin M, Orihovac Z, Mohammed AM. Perineural invasion by carcinoma of the lower lip. *J Craniomaxillofac Surg.* 1995;23:155-159.

45.   Gaddikeri S, Bhrany A, Anzai Y. Perineural invasion of skin cancers in the head and neck: an uncommon phenomenon revisited. *Otolaryngology.* 2014;4:2.

46.   Dercle L, Hartl D, Rozenblum-Beddok L, et al. Diagnostic and prognostic value of 18F-FDG PET, CT, and MRI in perineural spread of head and neck malignancies. *Eur Radiol.* 2018;28:1761-1770.

47.   Caldemeyer KS, Mathews VP, Righi PD, Smith RR. Imaging features and clinical significance of perineural spread or extension of head and neck tumors. *Radiographics.* 1998;18:97-110.

48.   Ginsberg LE. MR imaging of perineural tumor spread. *Neuroimaging Clin N Am.* 2004;14:663-677.

49.   Russo CP, Smoker WR, Weissman JL. MR appearance of trigeminal and hypoglossal

motor denervation. *AJNR Am J Neuroradiol.* 1997;18:1375-1383.

50.   Lee SH, Seo HG, Oh BM, Choi H, Cheon GJ, Lee SU. Increased (18)F-FDG uptake in the trapezius muscle in patients with spinal accessory neuropathy. *J Neurol Sci.* 2016;362:127-130.

51.   Fukui MB, Blodgett TM, Snyderman CH, et al. Combined PET-CT in the head and neck: part 2. Diagnostic uses and pitfalls of oncologic imaging. *Radiographics.* 2005;25:913-930.

52.   Sheikhbahaei S, Taghipour M, Ahmad R, et al. Diagnostic accuracy of follow-up FDG PET or PET/CT in patients with head and neck cancer after definitive treatment: a systematic review and meta-analysis. *AJR Am J Roentgenol.* 2015;205:629-639.

53.   Rodella L, Buffoli B, Labanca M, Rezzani R. A review of the mandibular and maxillary nerve supplies and their clinical relevance. *Arch Oral Biol.* 2012;57:323-334.

54.   Shankland WE. The trigeminal nerve. Part III: the maxillary division. *Cranio.* 2001;19:78-83.

55.   Shankland WE. The trigeminal nerve. Part II: the ophthalmic division. *Cranio.* 2001;19:8-12.

56.   Phillips CD, Bubash LA. The facial nerve: anatomy and common pathology. *Semin Ultrasound CT MR.* 2002;23:202-217.

57.   Moonis G, Cunnane MB, Emerick K, Curtin H. Patterns of perineural tumor spread in head and neck cancer. *Magn Reson Imaging Clin N Am.* 2012;20:435-446.

58.   Roncallo F, Turtulici I, Arena E, et al. Unilateral hypoglossal neuropathy: a pictorial essay. *Neuroradiol J.* 1998;11:849-864.

59.   Morani AC, Ramani NS, Wesolowski JR. Skull base, orbits, temporal bone, and cranial nerves: anatomy on MR imaging. *Magn Reson Imaging Clin N Am.* 2011;19:439-456.

60.   Khan S, Chang R. Anatomy of the vestibular system: a review. *NeuroRehabilitation.* 2013;32:437-443.

61.   Larson TC, Aulino JM, Laine FJ. Imaging of the glossopharyngeal, vagus, and accessory nerves. *Semin Ultrasound CT MR.* 2002;23:238-255.
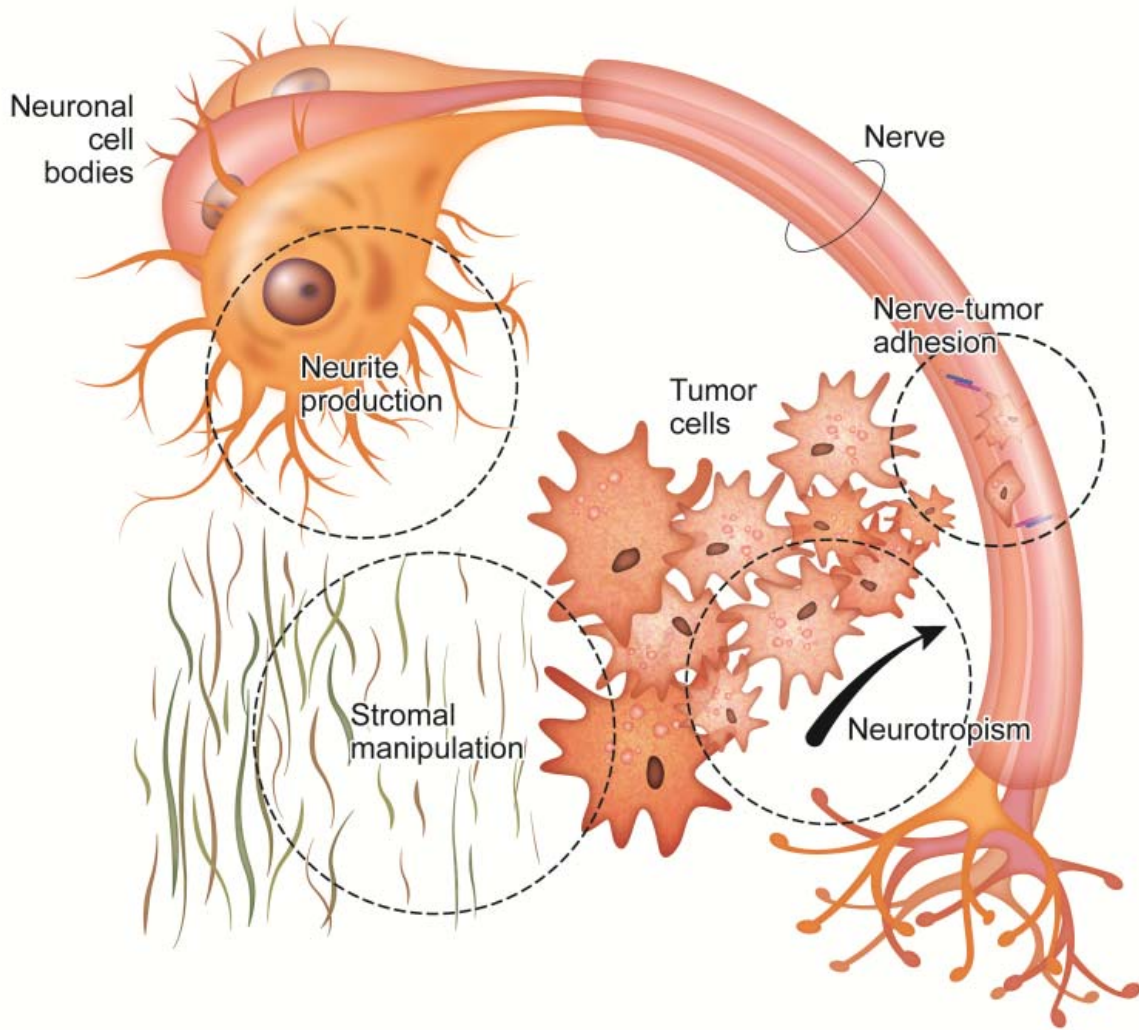
FIGURE 1. Functional outcomes of the biochemical mechanisms involved in perineural tumor growth. The connective stroma surrounding tumor cells is manipulated to facilitate perineural tumor spread, for example by matrix metalloproteinases. Nerve-tumor adhesion is achieved by membrane proteins such as neural cell adhesion molecule. Activation of nuclear transcription factors by various signaling molecules including nerve growth factor, brain-derived neurotrophic factor, glial cell-line derived neurotrophic factor, neurotrophin-3, and neurotrophin-4 contributes to stromal manipulation and nerve-tumor adhesion. It also leads to homing of tumor cells to nerves (neurotropism) and production of neurites to increase nerve-tumor contact. *(8,27)*
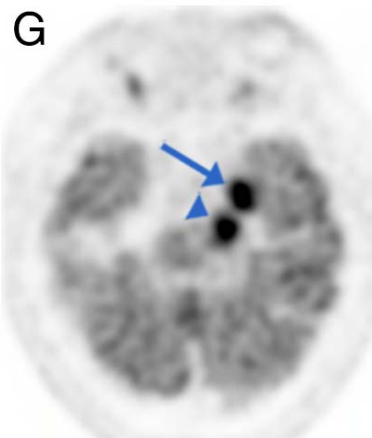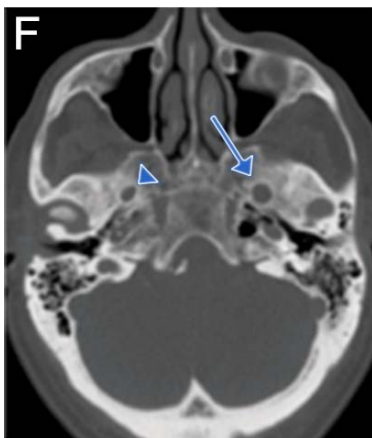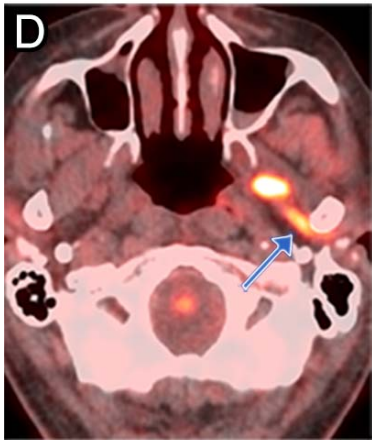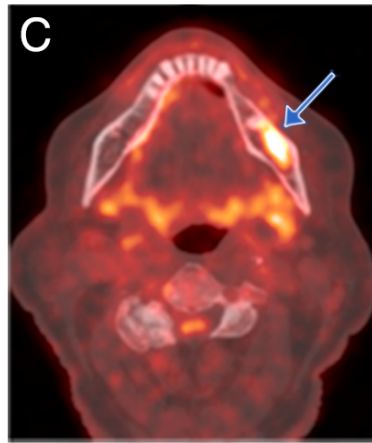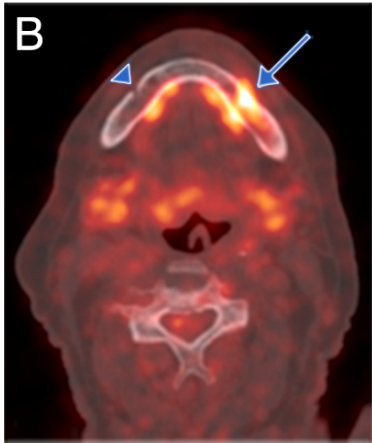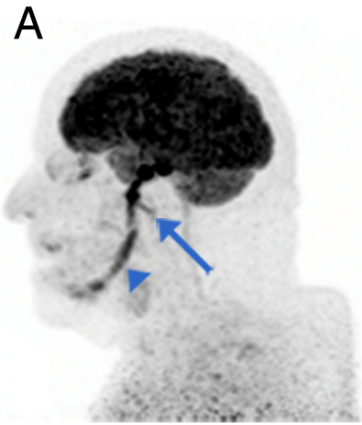
FIGURE 2. CN V3 (mandibular nerve - inferior alveolar and auriculotemporal branch) involvement in a patient with recurrent desmoplastic melanoma of the left lower lip presenting with left facial numbness. **(A)** Sagittal Maximum Intensity Projection (MIP) 18F-FDG PET image shows FDG-avid tumor spread along the entire course of the CN V3 (arrowhead) as well as along the auriculotemporal branch (arrow). Serial axial fused PET/CT images show FDG-avid tumor entry at the left mental foramen (arrow) in contrast to the normal right mental foramen (arrowhead) **(B)** and PNS along the inferior alveolar nerve through the mandibular canal (arrow) **(C),** along the auriculotemporal nerve (arrow) **(D),** and then cephalad through left foramen ovale (arrow) **(E)**, which is enlarged (arrow) compared to the normal contralateral side (arrowhead) on CT bone window **(F)**. Axial PET shows FDG-avid tumor spread cephalad to the trigeminal ganglion at Meckel's cave (arrow) and into the cisternal trigeminal nerve in the left prepontine cistern (arrowhead) **(G)**. The tumor was deemed inoperable in light of the intracranial perineural extension.
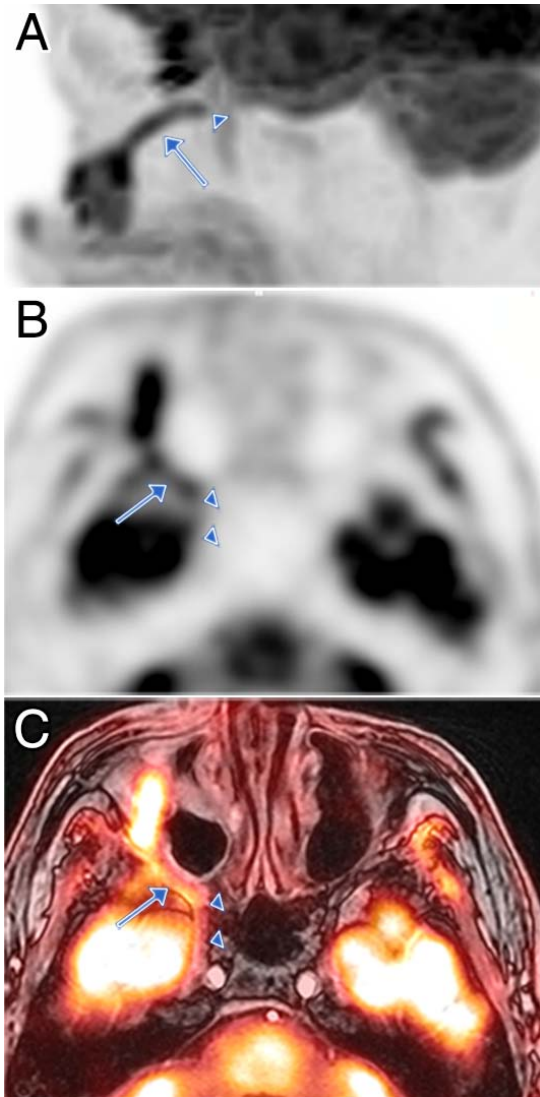
FIGURE 3. CN V2 (maxillary nerve - infraorbital branch) involvement in a patient with recurrent squamous cell carcinoma of the nose status-post multiple excisions including total rhinectomy and post-operative radiotherapy. Sagittal MIP 18F-FDG PET **(A)**, image shows FDG-avid tumor extension along the course of the right CN V2, originating from the tumor recurrence in the right cheek, tracking along the infraorbital nerve in the infraorbital canal (arrow), and entering the inferior orbital fissure into the region of the right pterygopalatine fossa (arrowhead). Axial PET **(B)** and axial fused PET/MR **(C)** images show PNS along the CN V2 past the pterygopalatine fossa (arrow) intracranially through right foramen rotundum (arrowheads) and into the inferior cavernous sinus. Tumor management required an aggressive local excision.
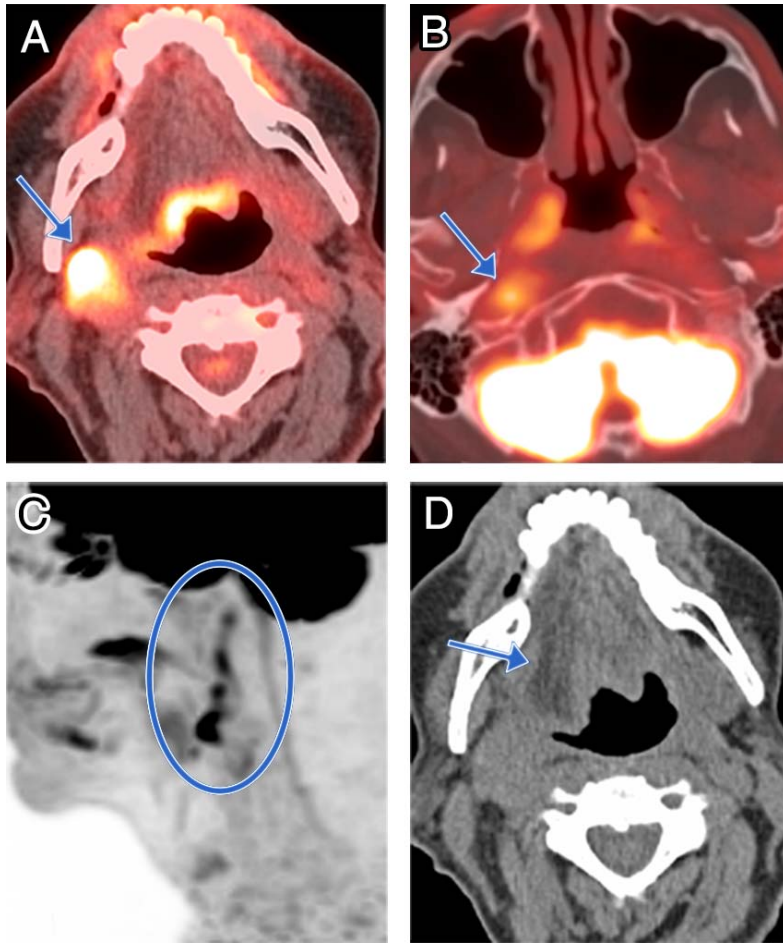
FIGURE 4. CN XII involvement in a patient with Stage IV metastatic squamous cell carcinoma from unknown primary, presenting with dysphagia and slurred speech. Axial fused 18F-FDG PET/CT images show FDG-avid metastatic tumor in the right carotid space (arrow) **(A)** and FDG-avid perineural tumor spread along the right CN XII superiorly to the base of skull just inferior to the hypoglossal canal **(B)**. **(C)** Sagittal MIP PET image shows the course of perineural tumor spread (circle). **(D)** Axial CT image shows ipsilateral right tongue atrophy with fatty infiltration (arrow) secondary to CN XII palsy. The patient subsequently received palliative radiation therapy of the neck mass.
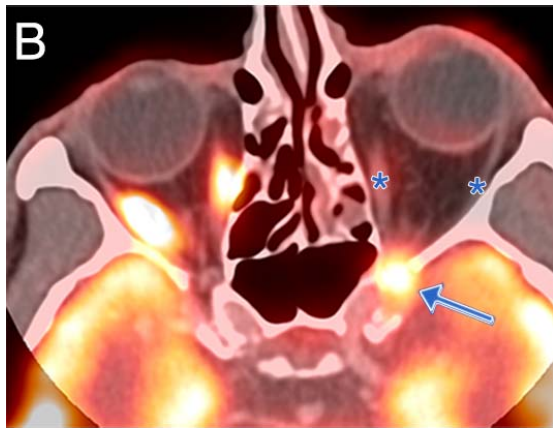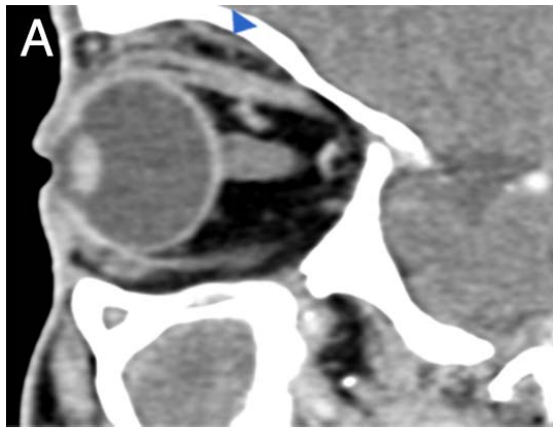
FIGURE 5. CNs V1, II, III, IV and VI involvement in a patient with basal cell carcinoma of the left eyebrow status-post resection, now presenting with progressive loss of left vision and inability to move the left eye. Sagittal CT **(A)**, axial fused 18F-FDG PET/CT **(B),** and coronal fused PET/CT **(C)** images of the left orbit show a cord of soft tissue in the superior extraconal space tracking along the course of left CN V1 (arrowhead) extending into the left orbital apex. A hypermetabolic

soft tissue mass in the left orbital apex (arrow) involves CN II, III, IV and VI resulting in vision

loss and denervation of left orbital extraocular muscles with atrophy and decreased FDG uptake

in the extraocular muscles (asterisks). Further surgical treatment was not pursued, as the PNS

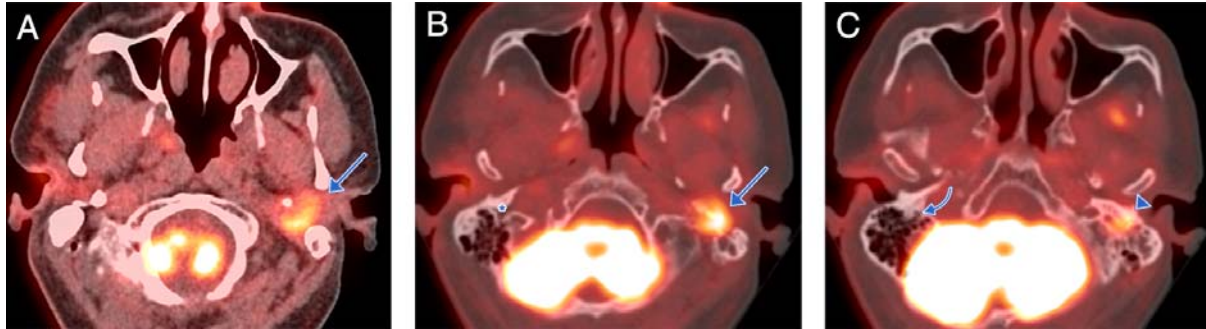would have required craniectomy and orbital exenteration.

FIGURE 6. CN VII involvement in a patient with myoepithelial carcinoma of the left parotid gland status-post parotidectomy and chemoradiation, now with tumor recurrence and left-sided preauricular pain, facial droop exacerbation, and metallic taste. Axial fused 18F-FDG PET/CT **(A)** image shows FDG-avid mass representing local tumor recurrence deep to the parotidectomy bed and anterior to the left mastoid tip (arrow). Axial fused PET/CT images **(B-C)** show FDG uptake extending cephalad from the parotid space through the stylomastoid foramen (arrow) into the facial canal in the left mastoid temporal bone (arrowhead) representing PNS along the mastoid segment of the CN VII, in comparison to contralateral normal stylomastoid foramen (asterisk) and facial canal (curved arrow). The recurrent tumor had partial treatment response with stereotactic radiosurgery.
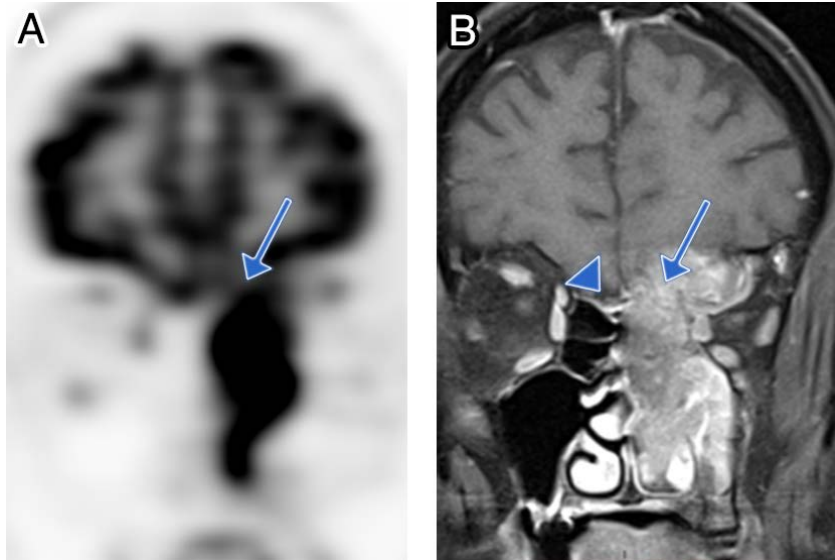
SUPPLEMENTAL TEXT
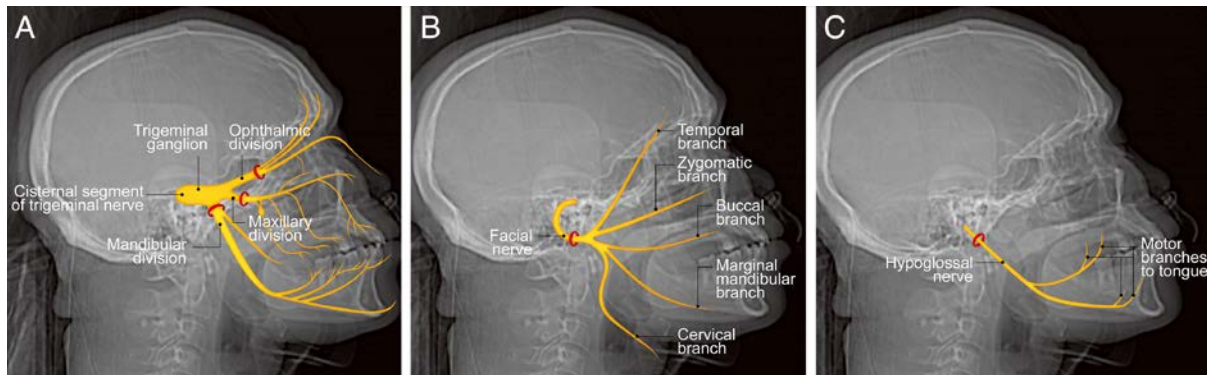
**SUPPLEMENTAL FIGURE 1.** Illustration of the nerves commonly involved in perineural spread. The trigeminal nerve and its three divisions **(A)**, the facial nerve and its five terminal motor branches **(B)**, and the hypoglossal nerve **(C)** are shown on a lateral skull radiograph.
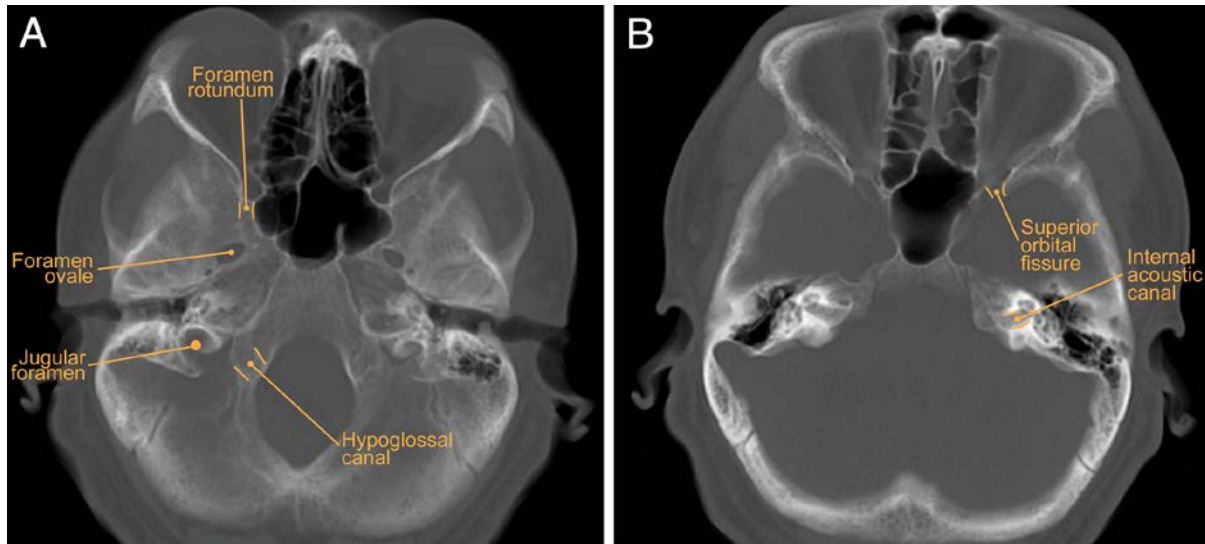
SUPPLEMENTAL FIGURE 2. Bony pathways used by the nerves commonly involved in perineural spread. The maxillary and mandibular divisions of the trigeminal nerve exit the skull through foramen rotundum and foramen ovale, respectively **(A)**. The facial nerve traverses the internal acoustic canal **(B)** before exiting the skull through the stylomastoid foramen. The ophthalmic division of the trigeminal nerve enters the orbit by via the superior orbital fissure **(B)**. The hypoglossal nerve travels through the hypoglossal canal **(A)** to enter the carotid space. The glossopharyngeal nerve, vagus nerve, and spinal accessory nerve enter the carotid space via the jugular foramen **(A)**.

SUPPLEMENTAL FIGURE 3. Cranial nerve I involvement in a patient with poorly differentiated carcinoma of the left sinonasal cavity and hypermetabolic tumor spread through the left cribriform plate (arrow) on coronal 18F-FDG PET image **(A).** Enhancing mass in the left sinonasal cavity invading through the left cribriform plate is seen with left olfactory bulb involvement (arrow) with normal right olfactory bulb (arrowhead) on coronal T1-weighted fat-suppressed post-contrast MRI **(B)**. The tumor was inoperable due to its extensive invasion into the surrounding structures.
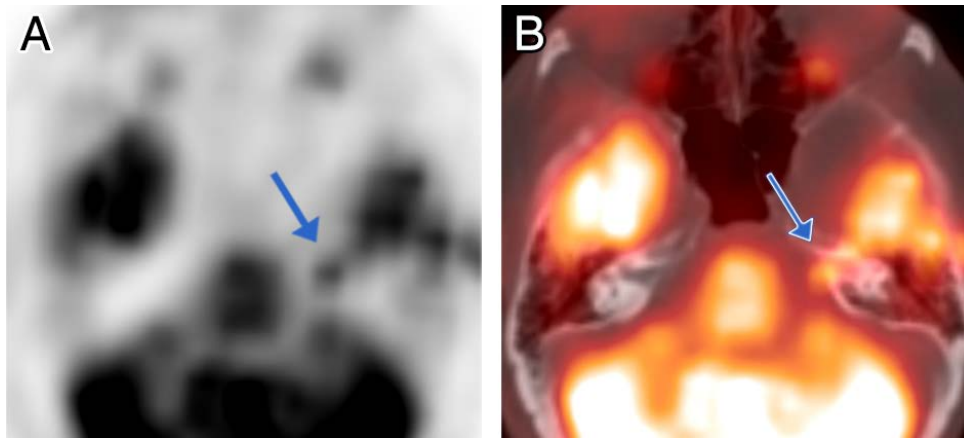
SUPPLEMENTAL FIGURE 4. Cranial nerve VIII involvement in a patient with high grade salivary duct carcinoma of the left parotid gland with perineural invasion into the left facial nerve and left facial weakness, status-post surgical excision and radiation therapy, now presenting with complete left-sided sensorineural hearing loss. Axial 18F-FDG PET **(A)** and axial fused PET/CT **(B)** images show abnormal focal radiotracer uptake in the left cerebellopontine angle extending into the left internal acoustic canal (arrow) representing tumor involvement along intracanalicular segment of CN VII. A presumed diagnosis of PNS along CN VIII was made with greater confidence given the location of abnormal FDG uptake and the sensorineural hearing loss.
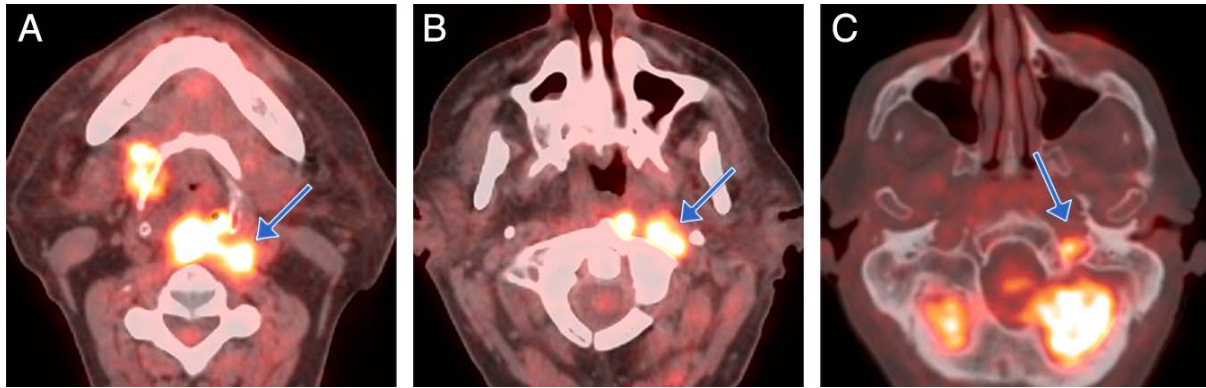
SUPPLEMENTAL FIGURE 5. Cranial nerves IX, X and/or XI involvement in a patient with poorly differentiated, locally advanced squamous cell carcinoma of the base of tongue status-post chemoradiation therapy, with local recurrence and persistent left-sided neck pain. Axial fused 18F-FDG PET/CT images show an FDG-avid posterior oropharyngeal wall mass extending into the prevertebral space and left retropharyngeal region (arrow) **(A)**, extending superiorly along the left carotid space (arrow) **(B)** into the left jugular foramen (arrow) **(C)**. Given the site of tumor recurrence as well spread along the course of the cranial nerves IX, X and XI in the carotid space and jugular foramen, PNS along one or more of the cranial nerves IX, X, and XI was suspected. The patient had concurrent distant metastatic disease and received palliative care.
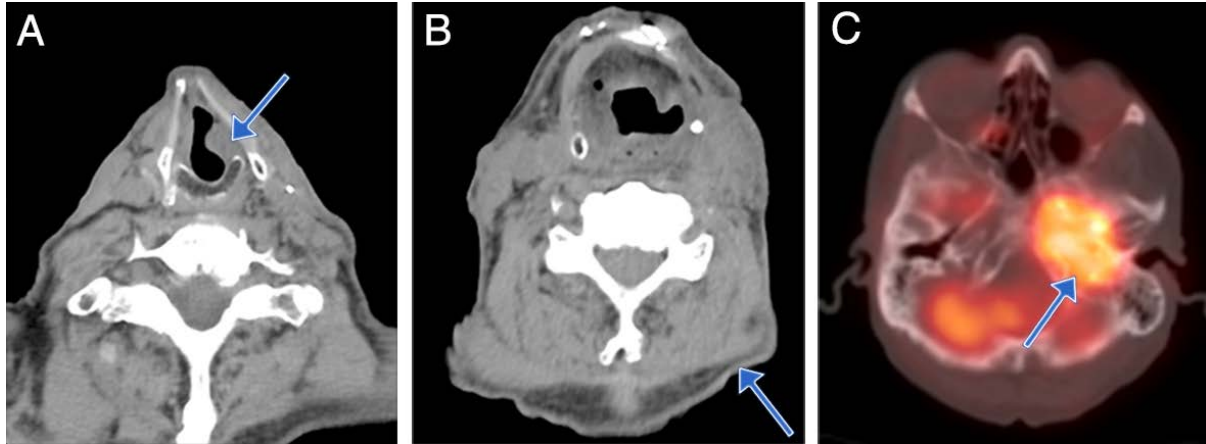
SUPPLEMENTAL FIGURE 6. Secondary signs/end-organ dysfunction from cranial nerve involvement by perineural spread of tumor on axial images taken from 18F-FDG PET/CT. A patient developed left vocal cord paresis (arrow) on axial CT **(A)** and left trapezius muscular atrophy (arrow) on axial CT **(B)** secondary to involvement of the left vagus (CN X) and spinal accessory nerves (CN XI), respectively, by a large FDG-avid tumor involving the left skull base including left jugular foramen on axial fused PET/CT (arrow) **(C)**. Asymmetric FDG uptake was not observed on the corresponding PET images due to the low physiologic uptake in these muscles in the resting state.

SUPPLEMENTAL TABLE 1.
Rates of perineural invasion in head and neck cancers by histologic type

	Histologic type	Rate of PNI	Incidence
Common neoplasms	Squamous cell carcinoma (mucosal)	14%-63% (*11*)	95% of non-cutaneous head and neck malignancies (*11*)
	oral cavity	63% (*11*)	25% of mucosal HNSCC (*12*)
	larynx & hypopharynx	36% (*13*)	34% of mucosal HNSCC (*12*)
	Squamous cell carcinoma (cutaneous)	2.5%-14% (*14*)	20% of non-melanoma skin cancers (*15*)
	Basal cell carcinoma	0.2%-3% (*16*)	80% of non-melanoma skin cancers (*15*)
	Mucoepidermoid carcinoma	29% (*17*)	30%-40% of salivary gland malignancies (*17*)
Neoplasms with high rates of PNI	Microcystic adnexal carcinoma	80% (*18*)	lifetime occurrence of less than one in a million (*19*)
	Desmoplastic melanoma	32% (*20*)	5% of melanoma cases (*20*)
	Adenoid cystic carcinoma	51%-56% (salivary) (*21*)	7.5%-10% of salivary gland malignancies (*21*)
		76% (cutaneous) (*22*)	0.23 case per one million person-years (*23*)

HNSCC: head and neck squamous cell cancer

SUPPLEMENTAL TABLE 2.
Primary tumor sites for cranial nerves commonly involved in perineural spread

	Cranial nerves	Tumor sites
Most commonly involved nerves	Facial (CN VII)	Parotid gland/adjacent skin, temporal bone/adjacent skin, external auditory canal, pterygopalatine ganglion
	Mandibular (CN V3)	Skin of lower lip and lower face, oral cavity, masticator space, oropharynx, nasopharynx, and parotid gland/adjacent skin
	Maxillary (CN V2)	Midfacial skin, upper lip, oral cavity, oropharynx, nasopharynx, nasal cavity, maxillary sinus, and palate
Less commonly involved nerves	Ophthalmic (CN V1)	Skin of upper face, orbit, lacrimal gland, frontal sinus, and ethmoid sinus
	Hypoglossal (CN XII)	Nasopharynx, tongue

SUPPLEMENTAL TABLE 3.
Clinical features and imaging findings of perineural spread along cranial nerves

| Associated signs and symptoms | Involved cranial nerve (CN) | Imaging findings | | Secondary sign: denervation injury |
| | | Primary sign: abnormality along the nerve | | |
		Location of abnormality	Key skull base bony landmarks	
Anosmia, abnormal taste	Olfactory (CN I)	Roof of nose, cribriform plate, anterior cranial fossa	Cribriform plate of ethmoid	
Visual loss	Optic (CN II)	Retrobulbar orbit, optic canal, suprasellar cistern	Optic canal	
Diplopia, ptosis, anisocoria	Oculomotor (CN III)	Superior orbital fissure, cavernous sinus, interpeduncular cistern	Superior orbital fissure	Extraocular muscles (except superior oblique and lateral rectus)
Vertical diplopia	Trochlear (CN IV)	Superior orbital fissure, cavernous sinus, ambient cistern	Superior orbital fissure	Superior oblique muscle
Paresthesia over forehead and upper eyelid, abnormal corneal reflex	Ophthalmic (CN V1)	Superior extraconal orbit, superior orbital fissure, cavernous sinus, Meckel's cave, prepontine cistern	Superior orbital fissure	
Paresthesia over upper cheek, upper lip, and posterior portion of nose	Maxillary (CN V2)	Infraorbital foramen, infraorbital canal, inferior orbital fissure, pterygopalatine fossa, foramen rotundum, cavernous sinus, Meckel's cave, prepontine cistern	Inferior orbital fissure, Foramen rotundum	
Paresthesia over chin and lower lip, trismus, abnormal jaw jerk reflex	Mandibular (CN V3)	Mental foramen, mandibular canal, masticator space/infratemporal fossa, foramen ovale, cavernous sinus, Meckel's cave, prepontine cistern	Foramen ovale	Masseter, medial and lateral pterygoid muscles
Lateral gaze diplopia	Abducens (CN VI)	Superior orbital fissure, cavernous sinus, prepontine cistern	Superior orbital fissure	Lateral rectus muscle
Hemiparesis of the upper and lower face	Facial (CN VII)	Parotid space, stylomastoid foramen, temporal bone, internal acoustic canal, cerebellopontine angle	Stylomastoid foramen	Facial muscles
Hearing loss, imbalance	Vestibulo-cochlear (CN VIII)	Internal auditory canal, cerebellopontine angle	Internal acoustic canal	
Absent gag reflex, glossopharyngeal neuralgia	Glosso-pharyngeal (CN IX)	Base of tongue and pharynx; carotid space; jugular foramen; cerebellomedullary cistern	Jugular foramen	
Dysphagia, hoarseness, vocal cord paralysis	Vagus (CN X)	Tracheoesophageal groove, carotid space, jugular foramen, cerebellomedullary cistern	Jugular foramen	Vocal cord, palatogossus muscle
Shoulder girdle depression,	Accessory (CN XI)	Posterior triangle of the neck, carotid space, jugular foramen,	Jugular foramen	Trapezius and sternocleidomastoid

inability to rotate head		cerebellomedullary cistern, foramen magnum		muscle
Dysarthria, dysphagia, tongue deviation	Hypoglossal (CN XII)	Tongue/floor of mouth, carotid space, hypoglossal canal, cerebellomedullary cistern	Hypoglossal canal	Extrinsic and intrinsic muscles of the tongue